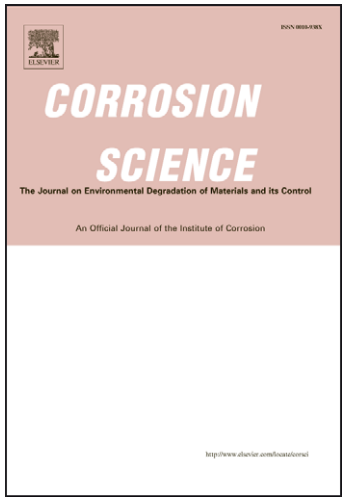

Brass Corrosion in Tap Water Distribution Systems Inhibited by Phosphate Ions

L. Yohai, M. Vázquez, M.B. Valcarce

PII: S0010-938X(10)00609-8
DOI: 10.1016/j.corsci.2010.12.005
Reference: CS 4230

To appear in: *Corrosion Science*

Received Date: 13 August 2010
Accepted Date: 11 December 2010

Please cite this article as: L. Yohai, M. Vázquez, M.B. Valcarce, Brass Corrosion in Tap Water Distribution Systems Inhibited by Phosphate Ions, *Corrosion Science* (2010), doi: 10.1016/j.corsci.2010.12.005

BRASS CORROSION IN TAP WATER DISTRIBUTION SYSTEMS INHIBITED BY PHOSPHATE IONS

L. Yohai, M. Vázquez and M.B. Valcarce*.

División Corrosión, INTEMA, Facultad de Ingeniería, UNMdP

Juan B. Justo 4302 - B7608FDQ Mar del Plata – Argentina

* corresponding author.
División Corrosión, INTEMA, Facultad de Ingeniería, UNMdP
Juan B. Justo 4302 - B7608FDQ Mar del Plata – Argentina
e-mail: mvalca@fi.mdp.edu.ar
Tel. : +54 223 481 6600 , Fax : +54 223 481 0046

November 24, 2010

Abstract

The effect of sodium orthophosphate on the protective characteristics of the surface layers are studied on brass in contact with moderately hard, highly carbonated and chloride rich simulated drinkable water. The optimal inhibitor concentration is evaluated from the composition, thickness and pitting resistance of the surface film. This layer is mainly composed by zinc(II) oxide-hydroxide and cuprous oxide. By adding PO_4^{3-}, the film quality improves, attributed to the incorporation of CuO or Zn(II) compounds. The changes are evident with 5 mg l^{-1} P, and between 10 and 20 mg l^{-1} P no significant differences are observed.

Key words :

A. brass ; B. cyclic voltammetry; C. pitting corrosion; C. passivity; C. neutral inhibition

1. Introduction

Aluminium brass is a copper-zinc alloy employed in domestic water-distribution systems in valves, heat exchangers, pumps, heating components, plumbing fittings and plumbing fixtures. The incorporation of zinc as alloying element improves the mechanical properties of these alloys and contributes in cost reduction. Furthermore, the addition of small amounts of aluminium to brass increases the resistance to corrosion in aqueous medium [1].

When the electrolyte allows the development of a compact oxide layer on the metal, the metallic surface is protected against general corrosion. However, under these conditions pitting corrosion could be a serious risk when chloride ions are present. In slightly alkaline solutions, brasses present lower pitting resistance than copper due to the incorporation of ZnO in the passive layer [2-5].

Sodium orthophosphate is used as corrosion inhibitor in tap water because in low concentrations it is innocuous for human consumption and has no negative impact on the environment [6]. This corrosion inhibitor acts by minimizing copper dissolution [7-12] and by decreasing the susceptibility to localized corrosion [13-15]. Also, Feng et al (1997), found a synergistic inhibitory effects of tripolyphosphate compounds on copper when zinc ions are present in tap water [16]. In addition, when phosphate ions are present in high concentrations, a delay in the anodic dissolution process on brass has been attributed to the development of a zinc phosphate layer [17, 18].

Mar del Plata is a coastal, Argentine city (lat. S:3756 – long. W:5735), where the drinkable water comes only from underground resources. This water is moderately hard and highly carbonated. Due to the marine intrusion of the coastal aquifers, the chloride

ions content is relatively high (not less than 100 mg l^{-1}). Argentine food-grade norms fix the upper limit for chloride ions content in 350 mg l^{-1} for drinkable water [19].

In this work, a solution that simulates moderately hard, highly carbonated and chloride rich drinkable water is used. Then, the effect of sodium orthophosphate on the protective characteristics of the surface layers, such us the composition, thickness and pitting resistance is studied on brass. In addition, to avoid water eutrophication when the drinkable water is wasted [20], it is important to determine the optimal inhibitor concentration.

2. Materials and methods

2.1. Electrodes preparation

Disc samples of aluminium brass (Cu 76%, Zn 22.18%, Al 1,8% and other impurities 0.02%) provided with appropriated back contacts were included in fast curing acrylic resin and mounted on polyvinyl chloride (PVC) holders. The geometrical area exposed was 0.785 cm^2. The electrodes were first abraded with emery paper and then mirror polished with 0.05 µm alumina powder (Type B–Buehler, Lake Bluff, USA). They were finally rinsed gently with distilled water.

2.2. Electrolyte composition

The experiments were carried out using artificial tap water (ATW) simulating the average composition of the drinkable water of an Argentine coastal city. The mineral base composition was $MgSO_4.7H_2O$ (40 mg l^{-1}), $MgCl_2.6H_2O$ (60 mg l^{-1}), KNO_3 (25 mg l^{-1}), $CaCl_2.H_2O$ (110 mg l^{-1}), Na_2CO_3 (470 mg l^{-1}) and $NaNO_3$ (20 mg l^{-1}) in distilled water; the pH was adjusted to 7.6 with 1 mol l^{-1} HCl. The final chloride ions concentration determined by potentiometric titration was 199 mg l^{-1} corresponding to

$[Cl^-]$= 5.6 mmol l^{-1}. The final conductivity of this water was 1.15 mS cm^{-1}, more than three times higher than the values reported for simulated water by other authors [16, 21-23]. When the conductivity of tap water is low, it can complicate electrochemical measurements, as it results in high solution resistance (R_s). However, it has been reported that in drinkable water this effect is important only for metals with high corrosion rates when the conductivity values are lower than of 0.1 mS cm^{-1}[24].

The dosages of orthophosphate tested were 5, 10 and 20 mg l^{-1} expressed as P, which correspond to 0.16, 0.32 and 0.64 mmol l^{-1} $NaH_2PO_4.H_2O$ respectively, using a 0.05 g ml^{-1} stock solution.

All the experiments were carried out at room temperature (20 ± 2 ºC).

2.3. Electrochemical techniques

The cell and instrumentation employed are standard and have been reported before [15]. A Luggin capillary minimized the ohmic drop, which together with the relatively high conductivity made unnecessary to compensate for ohmic drop.

All the potentials were indicated against the saturated calomel electrode (SCE).

Cyclic voltammograms were recorded after bubbling N_2 during 15 minutes. The electrodes were pre reduced in ATW at -1.15 V_{SCE} for 5 minutes. This pre treatment is meant to start from a reproducible, clean surface. Finally, the potential was scanned at 10 mV s^{-1}, starting at –1.15 V_{SCE} and reversing at a convenient potential that is indicated where relevant.

Passive films were grown at constant potentials on electrodes pre reduced in ATW at –1.15 V_{SCE} for 15 minutes. After that, the electrodes were immediately transferred to another cell where the oxides were investigated by potentiodynamic reductions in

deareated electrolyte. The potential was scanned at 10 mV s^{-1}. The starting point was the positive potential where the oxide had been grown. The scan ended at –1.15 V_{SCE}.

Polarization resistance (Rp), anodic polarization curves and electrochemical impedance spectra were evaluated on electrodes that were pre reduced at –1.15 V_{SCE} for 15 minutes and then kept at E_{corr} for 2 hours to stabilize the passive layer.

To record Rp, the potential was scanned ± 10 mV from E_{corr} at a 0.1 mV s^{-1}.

Anodic polarization curves were registered following the recommendations of ASTM [25], adapted for application to aluminum brass. The curves were registered potentiodynamicaly, from E_{corr} and using a sweep rate of 0.1 mV s^{-1}. The scan direction was reversed at 0.218 mA cm^{-2}, after attaining a convenient degree of attack.

Electrochemical impedance spectroscopy (EIS) tests were performed at E_{corr} applying an AC voltage signal of ± 10 mV_{rms} at a frequency between 20 kHz and 0.05 mHz. The solution was used without stirring or deareation. The results were fitted to the equivalent circuit presented in Fig. 1 using ZView™ [26]. This circuit, typical of oxide-coated metals, has been used before in relation to copper corrosion in potable water [22, 27, 28]. R_s represents the solution resistance between the electrode surface and the tip of the Luggin capillary, Z_{CPEo} a constant phase element related to the surface oxide, R_o the resistance to current flow through defects in the surface oxide, Z_{CPEdl} a constant phase element related to the double layer and R_{dl} the double layer resistance. The constant phase element (Z_{CPE}) is a non ideal capacitor and represents various types of non homogeneities typical of corroding electrodes. The impedance of this kind of elements is given by:

$$Z_{CPE} = [Q(j\omega)^n]^{-1} \quad (1)$$

where Q is a constant with dimensions of Ω^{-1} cm^{-2} s^n and n a constant power, with $-1<n<1$. Z_{CPE} can account for an inductance (n = -1), a resistance (n = 0), a Warburg impedance (n = 0.5) or a capacitance (n = 1).

2.4. UV-visible reflectance spectroscopy

The development of the passive film was also followed *in-situ*, by reflectance spectroscopy. This technique is useful to identify changes produced between 50 and 100 atomic layers in a semi-transparent solid [29].

The baseline was recorded polarizing two identical polished surfaces at –1.15 V_{SCE}. The spectroelectrochemical measurements were carried out in aerated electrolyte, using a Shimadzu UV 160A double-beam spectrophotometer, which was conveniently modified as described earlier [30, 31].

3. Results and discussion

The initial characterization of the system under investigation was carried out by recording cyclic voltammograms of brass at 10 mV s^{-1}. ATW and ATW with 5 and 10 mg l^{-1} P were used as electrolytes (see Fig. 2). In the absence of inhibiting ions, an increment in the anodic current at potentials higher than -0.2 V_{SCE} (Ia) and one anodic peak at –0.85 V_{SCE} (IIa) are evident. Localized corrosion initiates at potentials positive to -0.05 V_{SCE}. Two cathodic peaks appeared at –0.4 (Ic) and –1 V_{SCE} (IIc). Cathodic peak Ic could be assigned to the reduction of Cu(I) species, while peak IIc was attributed to the reduction of Zn(II) species [4, 28].

When 5 mg l^{-1} P were incorporated to the electrolyte, the intensity of the current increment at potentials higher than -0.2 V_{SCE} (Ia´) decreased and an ill-defined peak was present at -0.81 V_{SCE} (IIa´). In the negative direction, one broad peak was observed at

–0.33 V_{SCE} (I´c). Localized attack started when the potential exceeded 0 V_{SCE}. A similar response was observed when using 10 and 20 mg l^{-1} P: a current increment I´´a at potentials higher than –0.2 $V_{SCE,}$ an ill-defined peak at -0.77 V_{SCE} (IIa´´) and one broad cathodic peak at –0.38 V_{SCE} (I´´c). Localized attack initiation shifted in the positive direction and was now observed only at potentials higher than 0.15 V_{SCE}. The broad peak at –0.38 V_{SCE} resolved into two sharp cathodic peaks at -0.27 (I´´´c) and -0.37 V_{SCE} (II´´´c) with slower scans (figure 3), recorded at 1 mV s^{-1}. This suggests the incorporation of Cu(II) oxo-hydroxides to the surface film. The anodic sweep can be reverted at various different potentials so as to correlate anodic and cathodic peaks. No cathodic peaks can be seen if the scan direction is inverted at –0.4 V_{SCE} or more negative potentials.

The oxide layer formed at fixed potentials during 15 min on brass can also be characterized by potentiodynamic reduction curves (Fig. 4) and reflectance spectroscopy (Fig. 5). Fig. 4 shows that the oxide layer started to grow at potentials positive to –0.2 V_{SCE}. However, reflectance spectroscopy seems to be more sensitive, since a peak at 460 nm suggests the presence of Cu_2O in the spectrum obtained at -0.4 V_{SCE} (Fig. 5). The presence of Cu_2O at -0.4 V_{SCE} is not observed on pure copper [15]. In the case of brass, it could be related to the selective dissolution of Zn. As suggested before by other authors, dezincification might induce the formation of copper oxides at potentials that are more negative than those reported for pure copper [2]. In the spectra obtained at -0.4 V_{SCE} (Fig. 5) there is also a peak at 260 nm, which could be ascribed to zinc(II) oxide-hydroxides [4, 28, 32]. However, information on how to assign the peaks of Zn(II) phosphates or compounds other than oxides is not readily available in the bibliography.

When the surface film is grown 15 min at –0.2 V_{SCE}, only one cathodic peak appears at –0.38 V_{SCE} (Fig.4) which could be associated to Cu_2O reduction. The reflectance spectrum in this condition (Fig. 5) shows more intense absorbance peaks that, as above, can be attributed to Zn(II) compounds and to Cu_2O [29, 30]. Holding the potential at –0.1 V_{SCE} it could be seen that the charge associated to the reduction of Cu_2O (fig.4) is now higher. Similarly, an increment in the intensity of the absorbance is presented in Fig. 5. Both, the higher charge and the higher absorbance could be related to a thicker film.

At –0.050 V_{SCE}, the broad peak in the reduction curves (Fig. 4) started to resolve into two cathodic peaks at -0.35 and -0.45 V_{SCE}. The reflectance spectrum at this same potential showed that the relative intensity between peaks at 260 and 450 nm has changed. A similar response was observed holding the potential at 0.1 V_{SCE} but the current peaks in Fig. 4 were now present at -0.35 and -0.5 $V_{SCE.}$ The changes observed at potentials higher than -0.05 V_{SCE} could be attributed to the presence of CuO and higher quantities of Zn(II) compounds. Cupric oxide presents an absorption band in the near UV-region, superimposed to that absorption band corresponding to Zn(II) species. On other hand, a reduction peak associated to Zn(II) oxide-hydroxides was absent in Fig. 4 for all the potential values investigated. This might be due to the higher stability of $Zn_3(PO_4)_2$ (pK= 32) compared to ZnO or $Zn(OH)_2$ (pK=16.7) [18]. Probably, Zn(II) reduction from $Zn_3(PO_4)_2$ is not kinetically favoured within the range of cathodic sweep applied [16].

These results indicate that the surface film is mainly composed of Cu_2O, but as the potential moves in the positive direction the film might incorporate Zn(II) compounds and/or CuO, which cannot be distinguished.

Fig. 6 shows the potentiodynamic reduction of the layer grown during 2 hours at the E_{corr} in ATW with 0, 5 and 10 mg l^{-1} P. In ATW the features observed in the cyclic voltammogram remained: one peak associated to Cu_2O reduction at –0.74 V_{SCE} and other peak at –1.0 V_{SCE} associated to the reduction of Zn(II) oxide-hydroxides. When the inhibitor concentration is 5 mg l^{-1} P or higher, the charge related to the reduction of Cu_2O decreased markedly and one new cathodic peak appeared at –0.35 V_{SCE} which could be associated to CuO reduction. The substantial difference in the charge associated to the current peaks obtained with and without inhibitor suggests the development of a thinner surface film when brass is in contact with inhibited ATW. As discussed above for films anodically grown, the peak associated to the reduction of Zn(II) oxide-hydroxides is no longer present.

Fig. 7 presents the reflectance spectra of the oxides grown on brass after keeping it 2 hours at the E_{corr}. The presence of Cu_2O when brass is in contact with ATW can be confirmed by the absorbance peaks at 450 nm. There is also a peak at 260 nm that can be ascribed to Zn(II) oxo-hydroxides [4, 28, 32]. When 10 mg l^{-1} P is incorporated, the intensity of the absorption peaks decreased, as did the charge associated to the oxides reduction (fig. 6). These facts can again be correlated to the development of a thinner layer, in the presence of inhibitor. These changes, as before, can be attributed to the presence of a mixture of Zn(II) compounds, Cu_2O and CuO in the passive layer.

Impedance spectra recorded after applying a similar pre treatment are shown in Fig. 8, both as Nyquist (a) and Bode (b and c) plots. Fitting results are shown together with the recorded data. Two time constants can be seen, which are interpreted by means of the schematic representation of the structure of the surface film presented in Fig 1.

The experimental data were found to reasonably fit the equivalent circuit shown in Fig. 1. The optimised parameter values are presented in Table 1. When the inhibitor was

present, n_{dl} was fixed at 0.5 during the fitting procedure to simulate a Warburg element. This element can be associated to the diffusion of Cu(I) and Zn(II) ions through the surface film, which is the determining step in the corrosion process. The increment in the values of R_o and R_{dl} suggests that the passive layer growing on the surface in the presence of inhibiting ions is not only thinner (as shown when discussing Figs. 6 and 7) but also more compact [22]. Finally, the slight decrease in Q_0 cannot be used to estimate the thickness of the surface film since the chemisorption of phosphate ions will change the values of permittivity, as compared to those for massive CuO, Cu_2O and ZnO, which can be found in bibliography [33-35]. Also, thickness calculations are tricky since these are open porous structures impregnated with water, and the dielectric constant should be higher than that of a bulk oxide [36].

From the R_s values calculated for ATW (Table 1) it can also be confirmed that the ohmic drop is negligible. Given that R_s is 374 Ω cm^2 and taking 50 μA cm^2 as a representative value for the current density, the variation in the potential should be around 0.02 V, making unnecessary to perform further corrections.

Typical anodic polarization curves are presented in Fig. 9 for brass in ATW, ATW + 5 mg l^{-1} P and ATW + 10 mg l^{-1} P. The potential sweep was reversed when the current density reached 0.218 mA cm^{-2}. Using 20 mg l^{-1} P, the results resemble those for 10 mg l^{-1} P. Average values for the pitting potential (E_p), repassivation potential (E_{rp}) and corrosion potential (E_{corr}), from at least three independent experiments are shown in Table 2. It could be seen that when the inhibitor concentration increased, the pitting potential moved in the direction of more positive (noble) values. The difference (E_p – E_{corr}) was also higher. Interestingly enough, the difference between the repassivation potential and the corrosion potential (E_{rp} – E_{corr}) did not change noticeably. As the

inhibitor concentration increased, visual observation showed bigger and deeper pits, while the density of pits decreased (see Fig. 10).

When copper and brass behaviour in ATW are compared [4, 15], it could be seen that the presence of zinc as an alloying element moved the pitting potential towards less positive values. The difference ($E_p - E_{corr}$) was also higher for copper [4, 15]. The difference ($E_p - E_{corr}$) increases in 160 mV for brass and 218 mV for copper when 10 mg l^{-1} P was added to ATW [15]. Once the pitting process started, the repassivation process on brass was not favoured. This behaviour was similar to that observed on copper in ATW when PO_4^{3-} ions were present [15]. A higher ($E_p - E_{rp}$) difference could be associated to a more active dissolution process inside the pits [37]. In turn, this could be interpreted as a more difficult chemisorption of PO_4^{3-} on the bare brass substrate compared to chloride ions adsorption inside the pits [15, 37-40]. The presence of Zn(II) compounds in the passive layer could favour a different inhibition mechanism of PO_4^{3-} ions on brass than on copper.

The polarization resistance values measured in ATW, ATW + 5 mg l^{-1} P and 10 mg l^{-1} P are displayed in Table 3 taking R_{dl} from the impedance spectra (Rp_{EIS}), and also from potential sweeps in the vicinity of the E_{corr} (Rp_{sweep}). There is a good correlation between the values from both techniques. Polarization resistance increases in a factor of 3.5 when using 5 mg l^{-1} P and increases even more for higher inhibitor concentrations. A slight increment in the Rp values is observed for 10 mg l^{-1} P and no further variation is observed between 10 and 20 mg l^{-1} P. So, even when 5 mg l^{-1} P seems to be enough to increase the resistance to generalized corrosion, it has to be kept in mind that the resistance to pitting corrosion is optimal for 10 mg l^{-1} P. The higher values of the polarization resistance when the inhibitor is present can be associated to a greater

difficulty in the diffusion of Cu(I) and Zn(II) ions through the less porous, thinner and denser oxide film, which is the determining step in the corrosion process [21, 28].

4. Conclusions

The effect of phosphate ions on the nature of the passive layer that develops on brass in contact with moderately hard, highly carbonated and chloride-rich drinkable water has been analyzed using a variety of *in-situ* techniques.

The oxide layer is mainly composed by Zn(II) oxide-hydroxide and cuprous oxide. By adding PO_4^{3-} as corrosion inhibitor, the quality of the film improves, as it becomes less porous, thinner and denser. The incorporation of CuO to the passive layer or an increase in the amount of Zn(II) compounds could be responsible for this behaviour. The changes due to the presence of phosphate are evident even with the lower inhibitor dose tested (5 mg l^{-1} P), and between 10 and 20 mg l^{-1} P no significant differences are observed.

The polarization resistance markedly increases when 5 mg l^{-1} P of the inhibitor are added. A slight increment is observed using 10 mg l^{-1} P and no further variation is registered between 10 and 20 mg l^{-1} P. In comparison with the behaviour of copper in inhibited ATW [15], the incorporation of Zn as alloying element improves the resistance of brass to generalized corrosion, requiring a lower concentration of phosphate ions to obtain a similar behaviour.

It has also been demonstrated that the pitting potential is more positive in the presence of inhibitor, as a consequence of the inhibitor retarding the pit initiation. The optimal dosage tested is 10 mg l^{-1} P. However, there seems to be no effect on the repassivation process. Therefore, once initiated, it looks as if this type of inhibitor was unable to hinder pit growth. The incorporation of Zn as alloying element and the presence of

Zn(II) phosphate in the passive layer when the inhibitor is present could explain the different action mechanism of PO_4^{3-} ions on brass, as compared to copper.

Although the presence of Zn(II) compounds could be established using UV-visible reflectance spectroscopy, the presence of PO_4^{3-} ions in the passive film needs to be evaluated using different surface characterization techniques such as Raman or X-ray Phothoelectron spectroscopy. Only then, a possible mechanism to explain the effect of this inhibitor on brass could be proposed.

Acknowledgements

This work has been supported by the University of Mar del Plata (Grant 15/G225), as well as by the National Research Council (CONICET, PIP0661) and the Agencia Nacional de Promoción Científica y Tecnológica (PICT 6-34112). L. Yohai wishes to thank CIC, Argentina, for her fellowship.

References

[1] K. M. Ismail, S. S. El-Egamy and M. Abdelfatah, Effects of Zn and Pb as alloying elements on the electrochemical behavior of brass in borate solutions, J. Appl. Electrochem. 31 (2001) 663-670.

[2] J. Morales, G. T. Fernandez, P. Esparza, S. Gonzalez, R. C. Salvarezza and A. J. Arvia, A comparative study on the passivation and localized corrosion of [alpha], [beta], and [alpha] + [beta] brass in borate buffer solutions containing sodium chloride--I. electrochemical data, Corros. Sci. 37 (1995) 211.

[3] M. V. Rylkina, Y. I. Kuznetsov, M. V. Kalashnikova and M. A. Eremina, Brass depassivation in neutral chloride media, Protection of metals 38 (2002) 387-393.

[4] M. B. Valcarce, S. R. de Sanchez and M. Vazquez, Localized attack of copper and brass in tap water: The effect of Pseudomonas, Corros. Sci. 47 (2005) 795-809.

[5] T. Kosec, I. Milosev and B. Pihlar, Benzotriazole as an inhibitor of brass corrosion in chloride solution, Appl. Surf. Sci. 253 (2007) 8863-8873.

[6] M. M. Critchley, N. J. Cromar, N. C. McClure and H. J. Fallowfield, The influence of the chemical composition of drinking water on cuprosolvency by biofilm bacteria, J. Appl. Microbiol. 94 (2003) 501-507.

[7] M. Edwards, L. Hidmi and D. Gladwell, Phosphate inhibition of soluble copper corrosion by-product release, Corros. Sci. 44 (2002) 1057-1071.

[8] S. O. Pehkonen, A.Palit and X. Zhang, Effect of specific water quality parameters on copper corrosion, Corros. 58 (2002) 156-165.

[9] Y. Zhe and S. O. Pehkonen, Copper corrosion kinetics and mechanisms in the presence of chlorine and orthophosphate, Water Scie. Technol. 49 (2004) 73-81.

[10] S. Li, L. Ni, C. Sun and L. Wang, Influence of organic matter on orthophosphate corrosion inhibition for copper pipe in soft water, Corros. Sci. 46 (2004) 137-145.

[11] N. Soussi and E. Triki, A chemiometric approach for phosphate inhibition of copper corrosion in aqueous media, J. Mater. Sci. 42 (2007) 3259-3265.

[12] N. Souissi and E. Triki, Modelling of phosphate inhibition of copper corrosion in aqueous chloride and sulphate media, Corros. Sci. 50 (2008) 231-241.

[13] M. Drogowska, L. Brossard and H. Menard, Comparative study of copper behaviour in bicarbonate and phosphate aqueous solutions and effect of chloride ions, J. Appl. Electrochem. 24 (1994) 344-349.

[14] D. Lytle and M. N. Nadagouda, A comprehensive investigation of copper pitting corrosion in a drinking water distribution system, Corros. Sci. 52 (2010) 1927-1938.

[15] M. B. Valcarce and M. Vázquez, Phosphate ions used as green inhibitor against copper corrosion in tap water, Corros. Sci. 52 (2010) 1413–1420.

[16] Y. Feng, K. S. Siow, W. K. Teo, K. L. Tan and A. K. Hsieh, Synergistic effects between sodium tripolyphosphate and zinc sulfate in corrosion inhibition of copper in neutral tap water, Corros. 53 (1997) 546-555.

[17] E. A. Ashour and B. G. Ateya, The effect of phosphates on the susceptibility of alfa-brass to stress corrosion cracking in sodium nitrite, Corros. Sci. 37 (1995) 371-380.

[18] G. Kilincceker and E. Mehmet, The effect of phosphate ions on the electrochemical behaviour of brass in sulphate solutions, Mater. Chem. Phys. 119 (2009) 30-39.

[19] Código Alimentario Argentino, Capítulo XII, artículo 982, Bs. As., Argentina, Ley 18284.

[20] M. Salasi, T. Shahrabi, E. Roayaei and M. Aliofkhazraei, The electrochemical behaviour of enviroment-friendly inhibitors of silicate and phosphonate in corrosion control of carbon steel in soft water media, Mater. Chem. Phys. 104 (2007) 183-190.

[21] Y. Feng, W. K. Teo, K. S. Siow, K. L. Tan and A. K. Hsieh, The corrosion behaviour of copper in neutral tap water. Part I: Corrosion mechanism, Corros. Sci. 38 (1996) 369-385.

[22] A. Palit and S. Pehkonen, Copper corrosion in distribution systems: evaluation of a homogeneous Cu_2O film and a natural corrosion scale as corrosion inhibitors, Corros. Sci. 42 (2000) 1801-1822.

[23] S. H. Lee, J. G. Kim and J. K. Koo, Investigation of pitting corrosion of a copper tube in a heting system, Engin. Fail. Analysis 17 (2010) 1424-1435.

[24] Internal corrosion of water distribution systems, American Water Works Association (AWWA), Denver, USA, 1996.

[25] American Society of Testing and Materials, ASTM G61-86, Philadelphia, 1993.

[26] Zplot for windows, I. Scribner Associates, 1998.

[27] J. Shim and J. Kim, Copper corrosion in potable water distribution systems: influence of copper products on the corrosion behavior, Mater. Let. 58 (2004) 2002-2006.

[28] M. B. Valcarce, S. R. de Sanchez and M. Vazquez, A comparative analysis of copper and brass surface films in contact with tap water, J. Mater. Sci. 41 (2006) 1999-2007.

[29] R. E. Hummel, Differential Reflectometry and Its Application to the Study of Alloys, Phys. State Sol. (a) 76 (1983) 12-43.

[30] S. R. de Sanchez, L. E. A. Berlouis and D. J. Schiffrin, Difference Reflectance Spectroscopy of Anodic Films on Copper and Copper Base Alloys, Journal of Electroanal. Chem. 307 (1991) 73-86.

[31] S. Cere and M. Vazquez, Properties of the passive films present on copper and copper- nickel alloys in slightly alkaline solutions, J. Mater. Sci. Lett. 21 (2002) 493-495.

[32] B. S. Kim, T. Piao, S. N. Hoier and S. M. Park, In situ spectro-electrochemical studies on the oxidation mechanism of brass, Corros. Sci. 37 (1995) 557.

[33] Y. V. Ingelgem, A. Hubin and J. Vereecken, Investigation of first stages of localized corrosion of pure copper combining EIS, FE-SEM and FE-AES, Electrochim. Acta 52 (2007) 7642-7650.

[34] M. Metikos-Hukovic, R. Babic and I. Paic, Copper corrosion at various pH values with and without the inhibitor, J. Appl. Electrochem. 30 (2000) 617-624.

[35] Handbook of Chemistry and Physics, NY, 1998.

[36] M. J. Esplandiu, E. M. Patrito and V. A. Macagno, Characterization of hafnium anodic oxide films: an AC impedance investigation, Electrochim. Acta 40 (1995) 809-815.

[37] M. Yamaguchi, H. Nishihara and K. Aramaki, The inhibition of pit growth on an iron surface in borate buffer solution containing chloride ion by inhibitors classified as soft bases in the HSAB principle, Corros. Sci. 37 (1995) 571.

[38] M. B. Valcarce and M. Vazquez, Carbon steel passivity examined in alkaline solutions: The effect of chloride and nitrite ions, Electrochim. Acta 53 (2008) 5007-5015.

[39] M. B. Valcarce and M. Vázquez, Carbon steel passivity examined in solutions with a low degree of carbonation: The effect of chloride and nitrite ions, Mater. Chem. Phys. 115 (2009) 313-321.

[40] V. S. Sastri, Corrosion inhibitors, John Wiley and Ltd., West Sussex, England, 1998.

Figure captions

Figure 1. Equivalent circuit proposed to fit the experimental data when two time constants are present.

Figure 2. Cyclic voltammograms of brass in deaerated ATW (—), ATW + 5 mg l^{-1} P (—○—) and ATW + 10 mg l^{-1} P (—□—). Scan rate: 10 mV s^{-1}.

Figure 3. Cyclic voltammogram of brass in deaerated ATW + 10 mg l^{-1} P. Scan rate: 1 mV s^{-1}.

Figure 4. Potentiodynamic reduction curves for oxides grown on brass at –0.4 V_{SCE} (—), –0.2 V_{SCE} (—○—), –0.1 V_{SCE} (—Δ—), -0.050 V_{SCE} (—*—) and 0.1 V_{SCE} (—□—) for 15 minutes in ATW + 10 mg l^{-1} P. Scan rate: 10 mV s^{-1}. Scan starts at growth potential.

Figure 5. Reflectance spectra for oxides grown on brass at –0.4 V_{SCE} (—), –0.2 V_{SCE} (—○—), –0.1 V_{SCE} (—Δ—), -0.05 V_{SCE} (—*—) and 0.1 V_{SCE} (—□—) for 15 minutes in ATW + 10 mg l^{-1} P.

Figure 6. Potentiodynamic reduction curves for oxides grown on brass in ATW (——), ATW + 5 mg l^{-1} P (—○—) and ATW + 10 mg l^{-1} P (—□—) after 2 hours at E_{corr}. Scan rate: 10 mV s^{-1}.

Figure 7. Reflectance spectra for oxides grown on brass in ATW (——) and ATW + 10 mg l^{-1} P (—□—) after 2 hours at E_{corr}.

Figure 8. Impedance spectra recorded on brass electrodes held for 2 hours at E_{corr} in ATW (—Δ—), ATW + 5 mg l^{-1} P (—○—) and ATW + 10 mg l^{-1} P (—□—). The symbols represent the data and the lines the fitting results. (a) Nyquist representation; (b) and (c) Bode representation.

Figure 9. Anodic polarization curves for brass in ATW (——), ATW + 5 mg l^{-1} P (—○—) and ATW + 10 mg l^{-1} P (—□—). The curves are recorded after holding the electrodes 2 hours at E_{corr} and each started at E_{corr}. Scan rate: 0.1 mV s^{-1}.

Figure 10. Micrographs of the electrodes surface after performing anodic polarization curves. a) ATW, b) ATW + 5 mg l^{-1} P and c) ATW + 10 mg l^{-1} P.

Figure 1

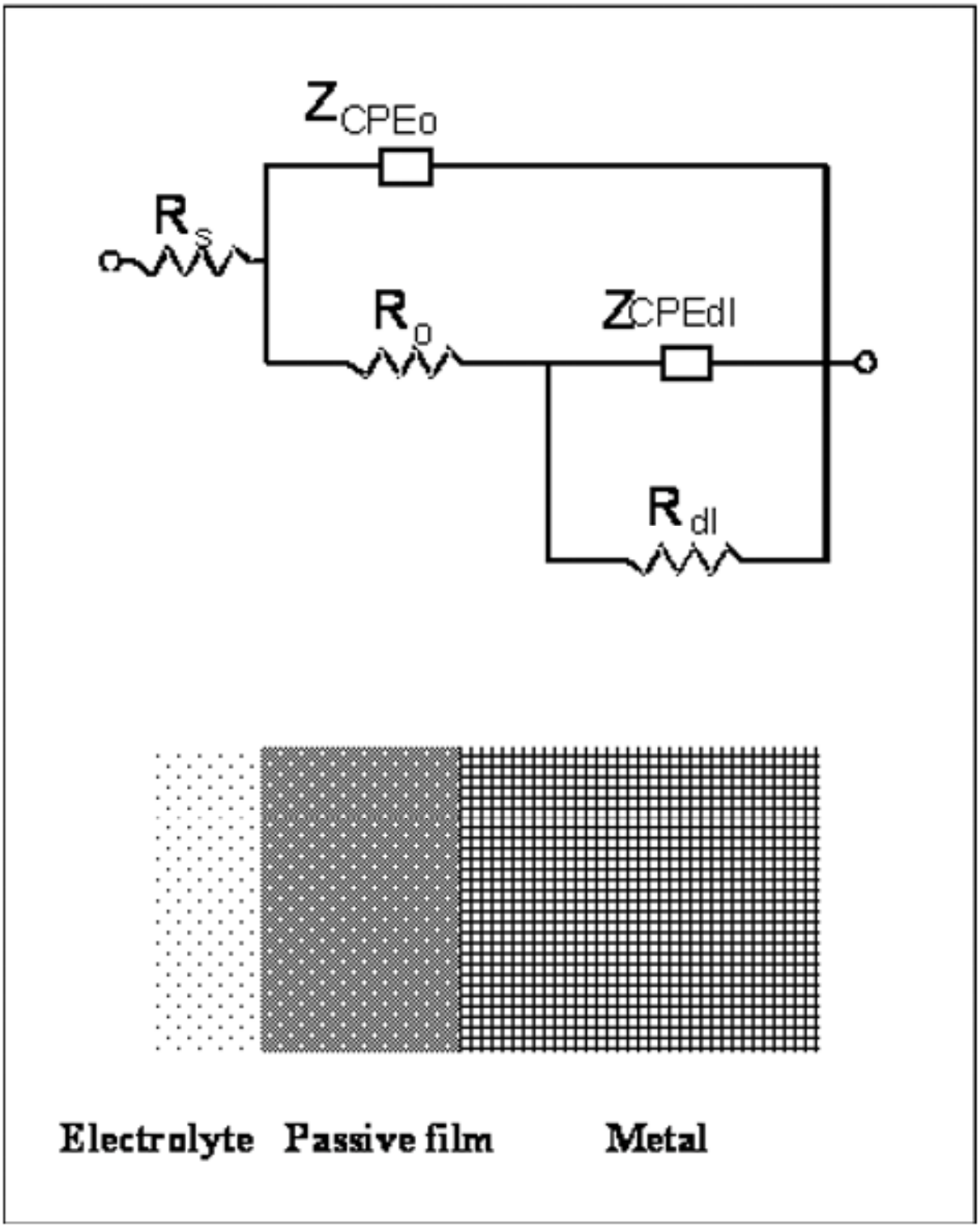

Figure 2

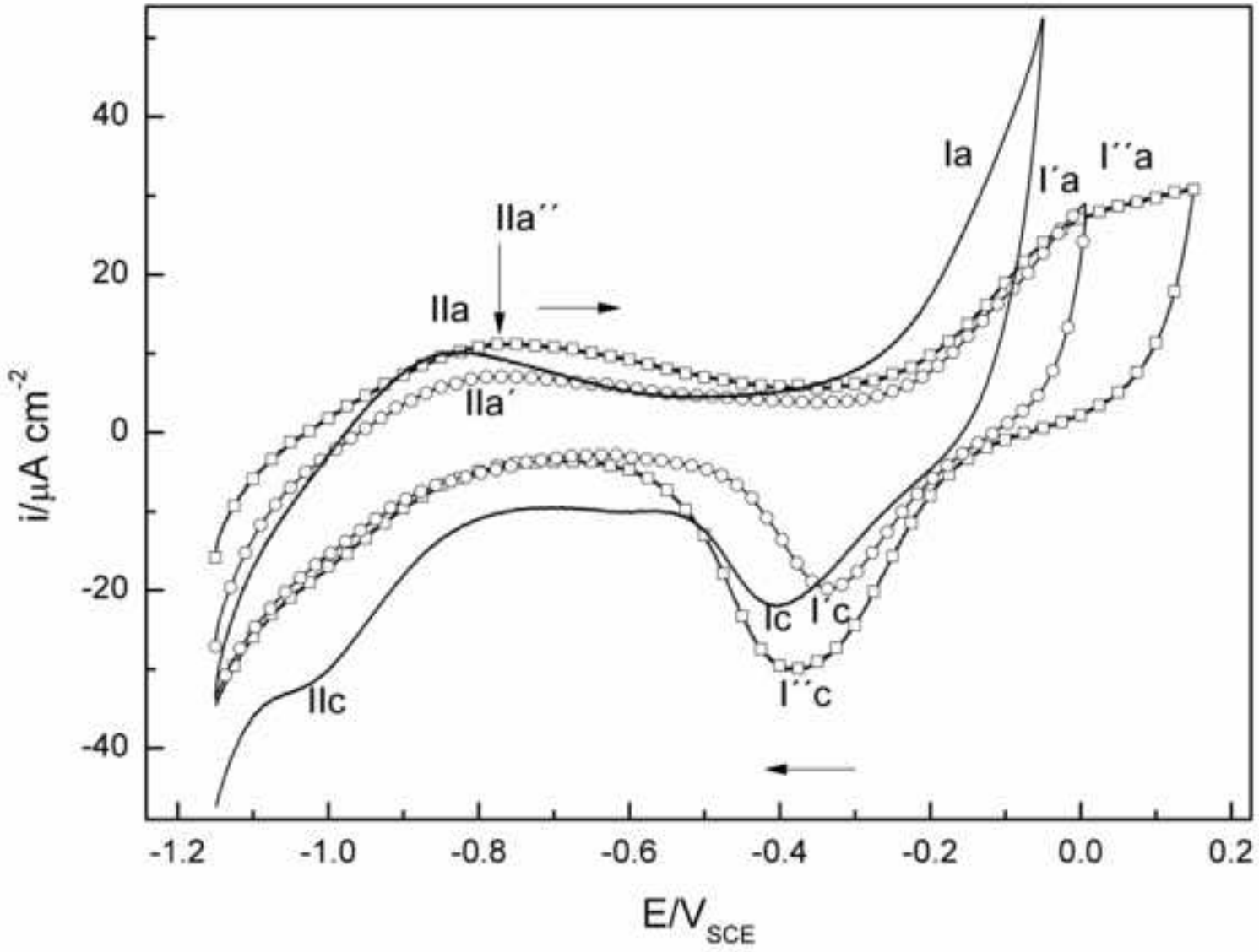

Figure 3

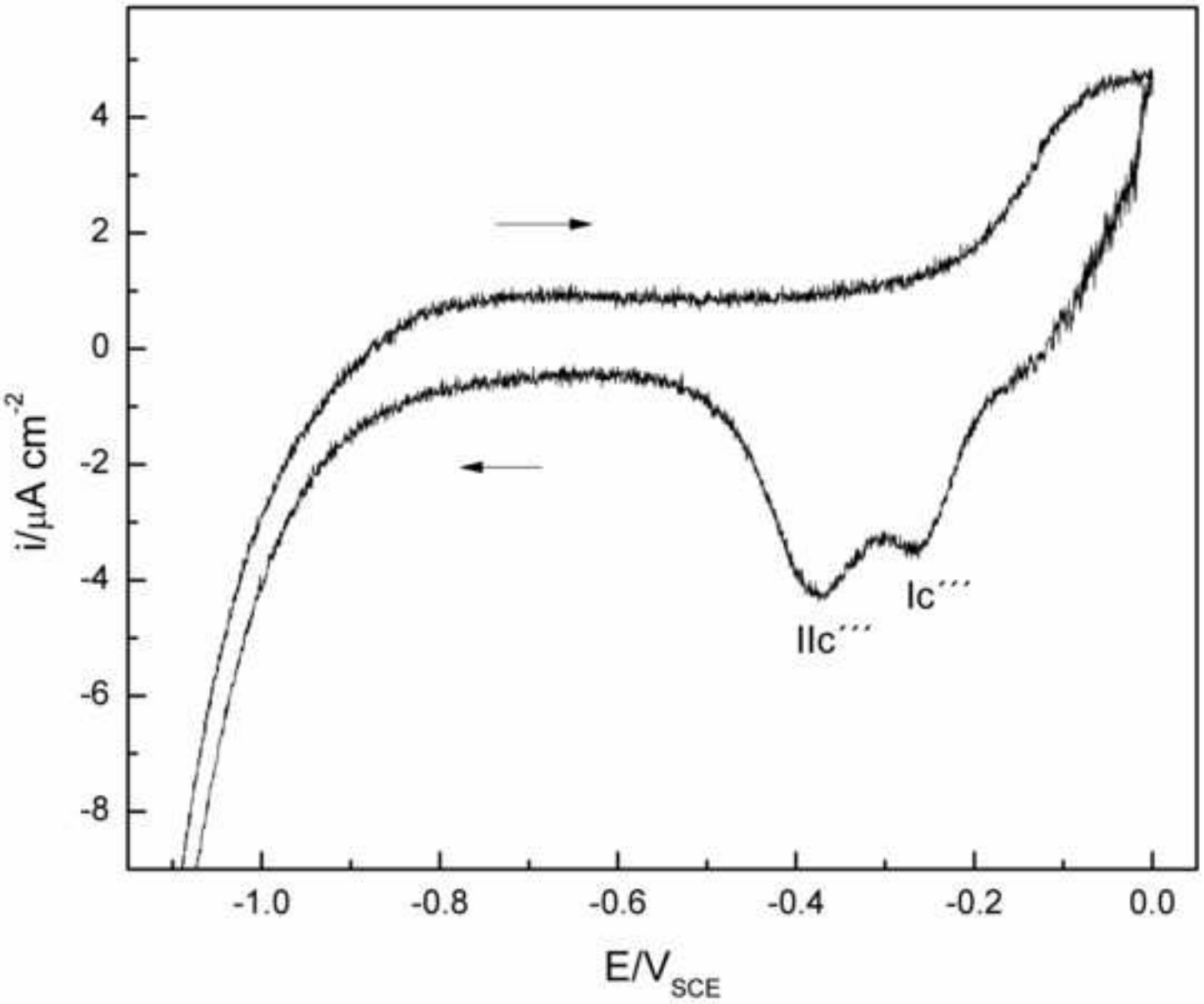

Figure 4

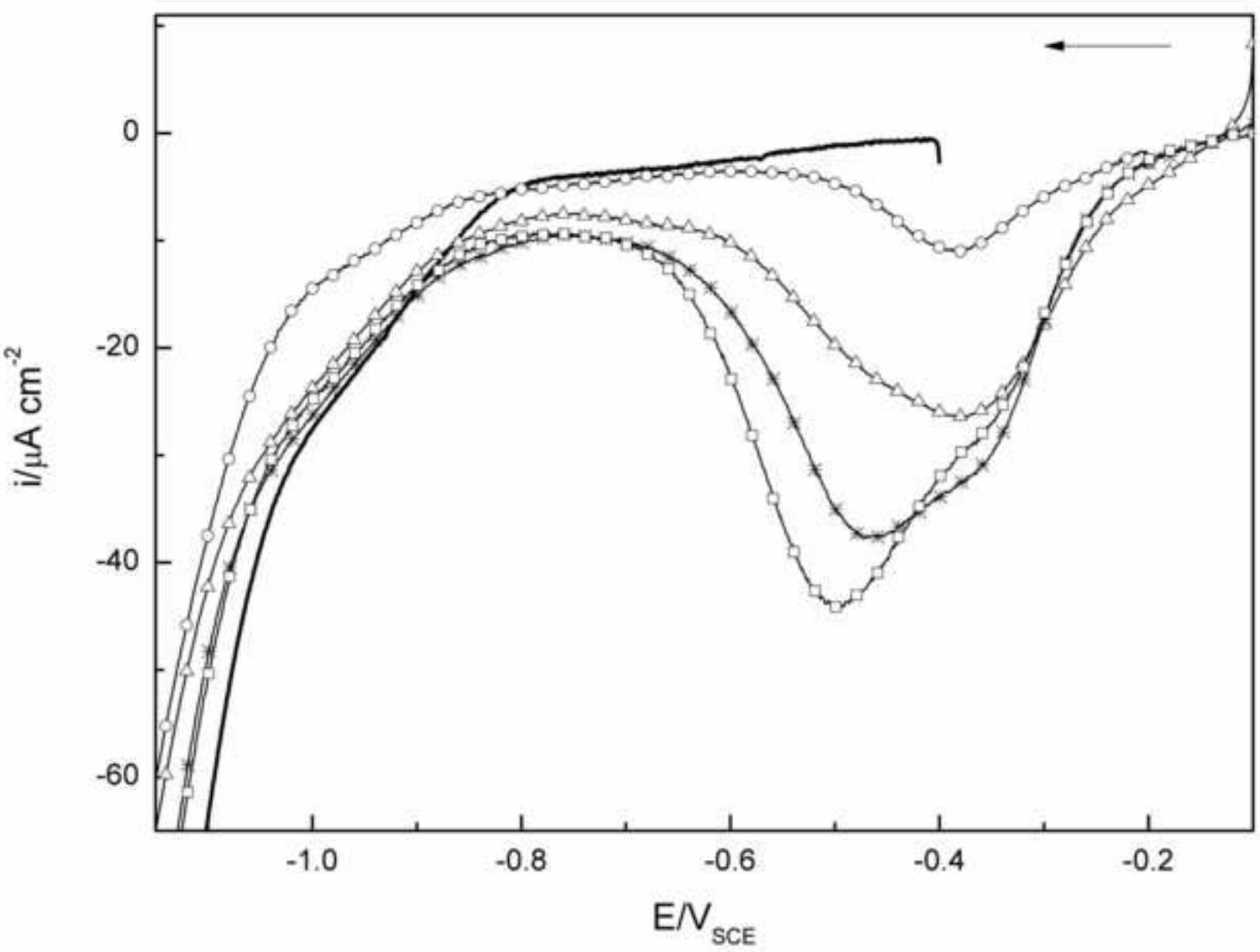

Figure 5

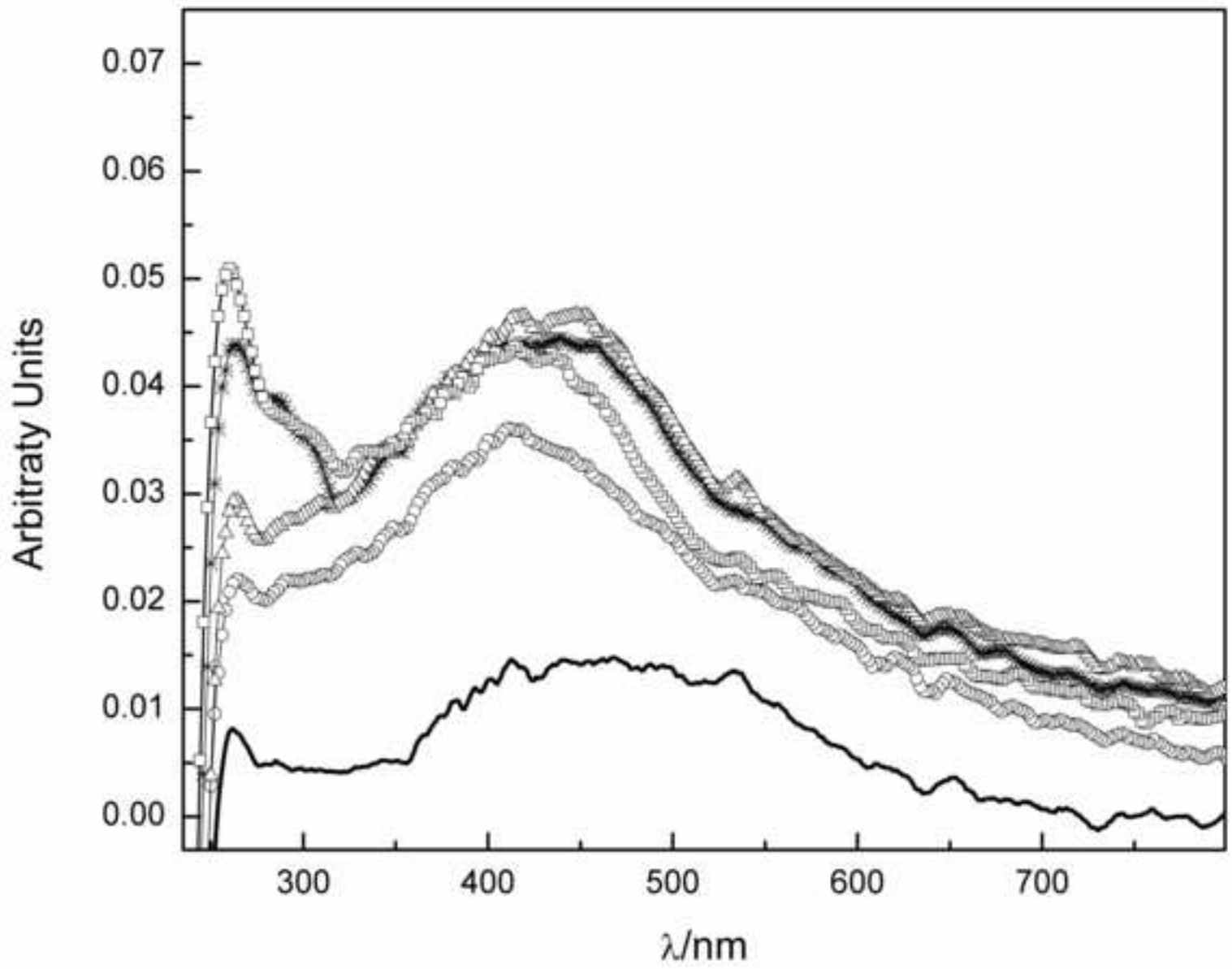

Figure 6

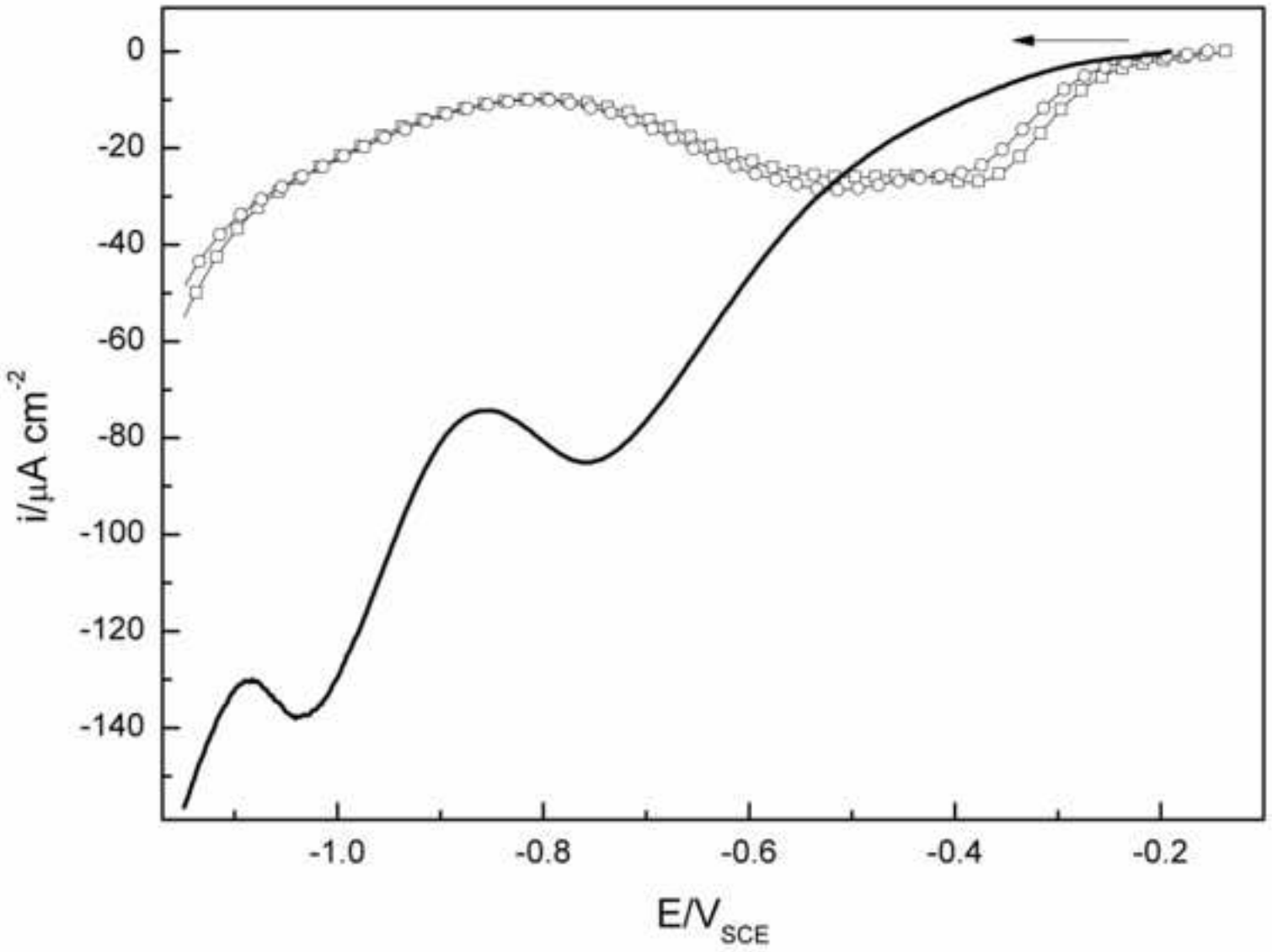

Figure 7

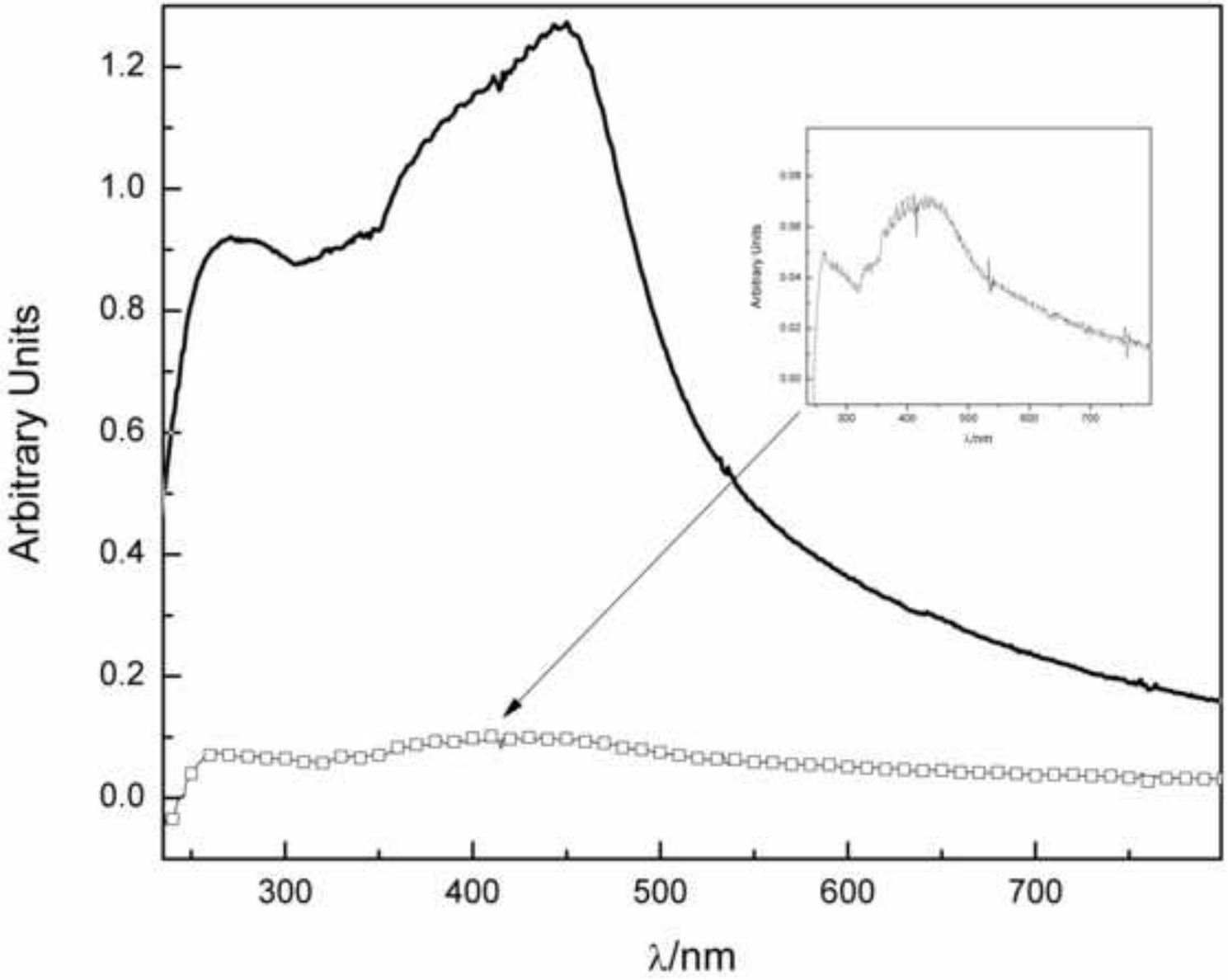

Figure 8a

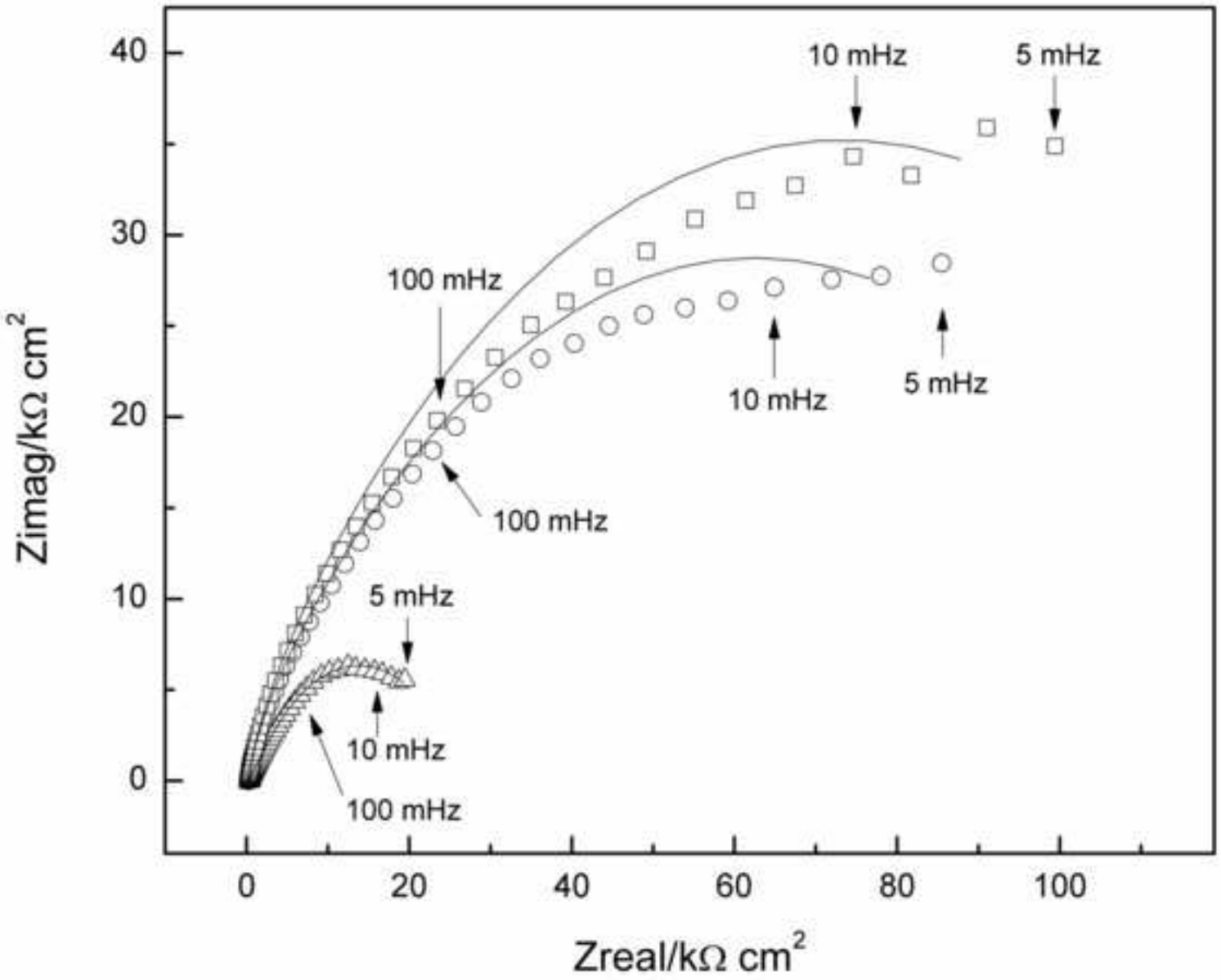

Figure 8b

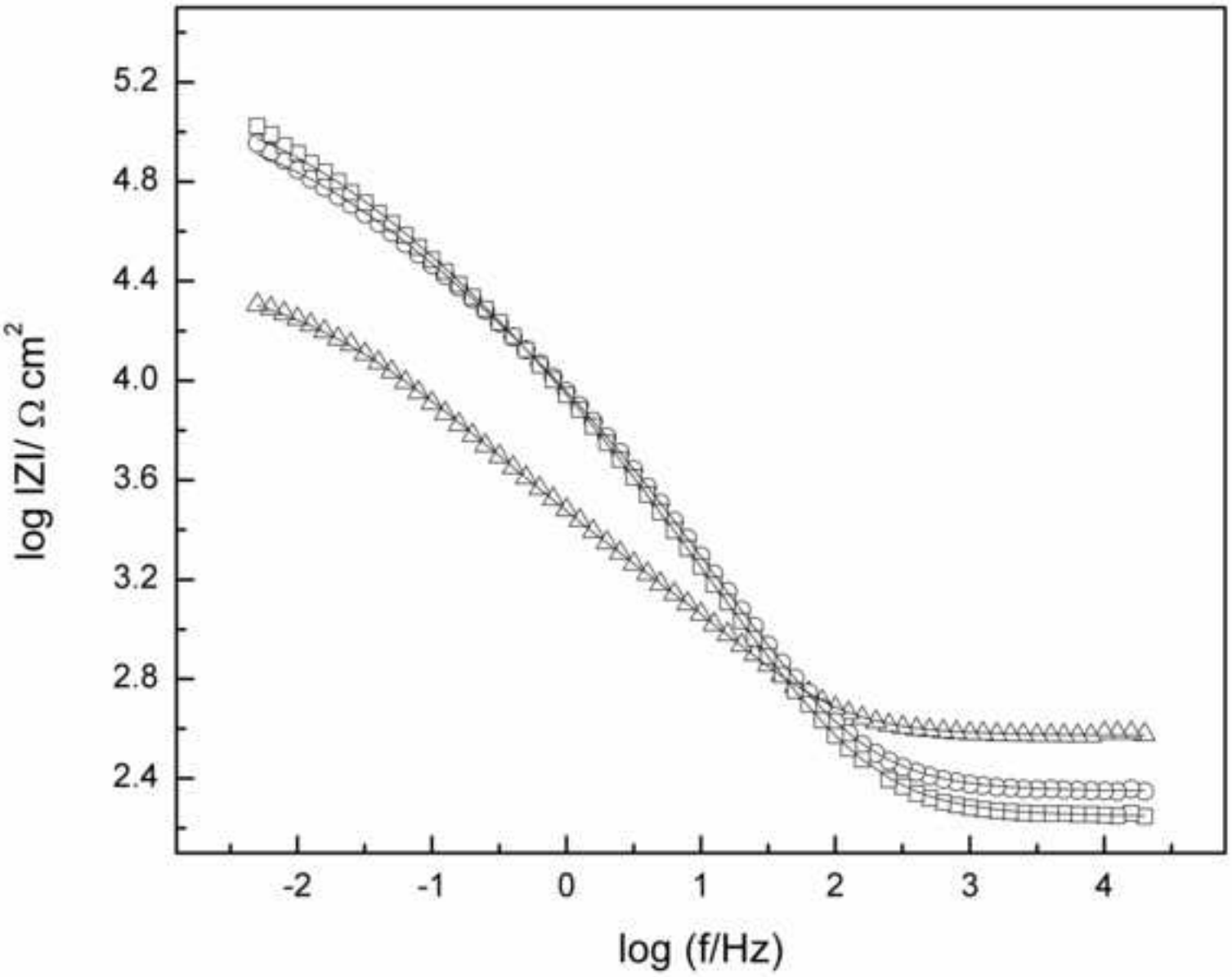

Figure 8c

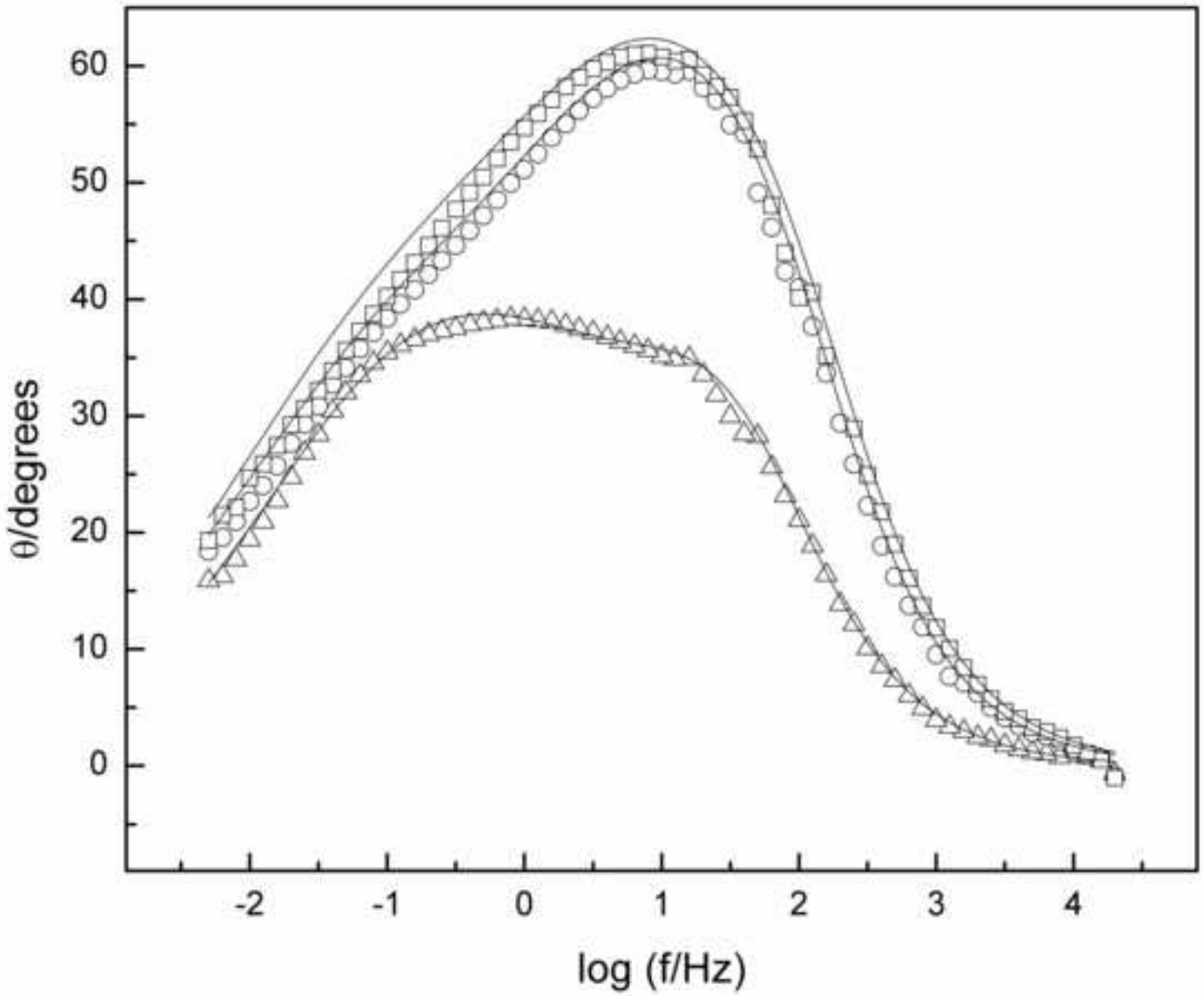

Figure 9

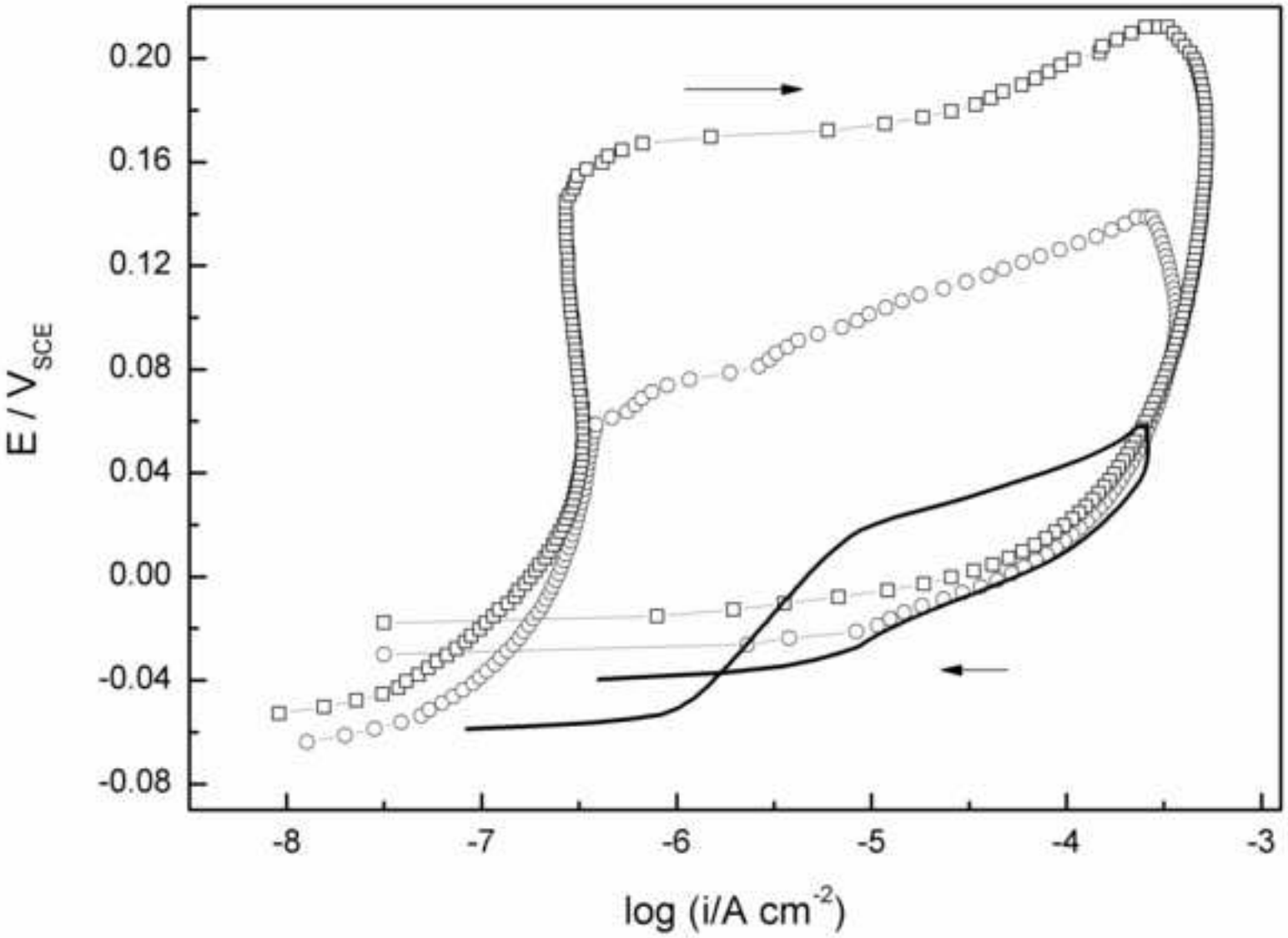

Figure 10

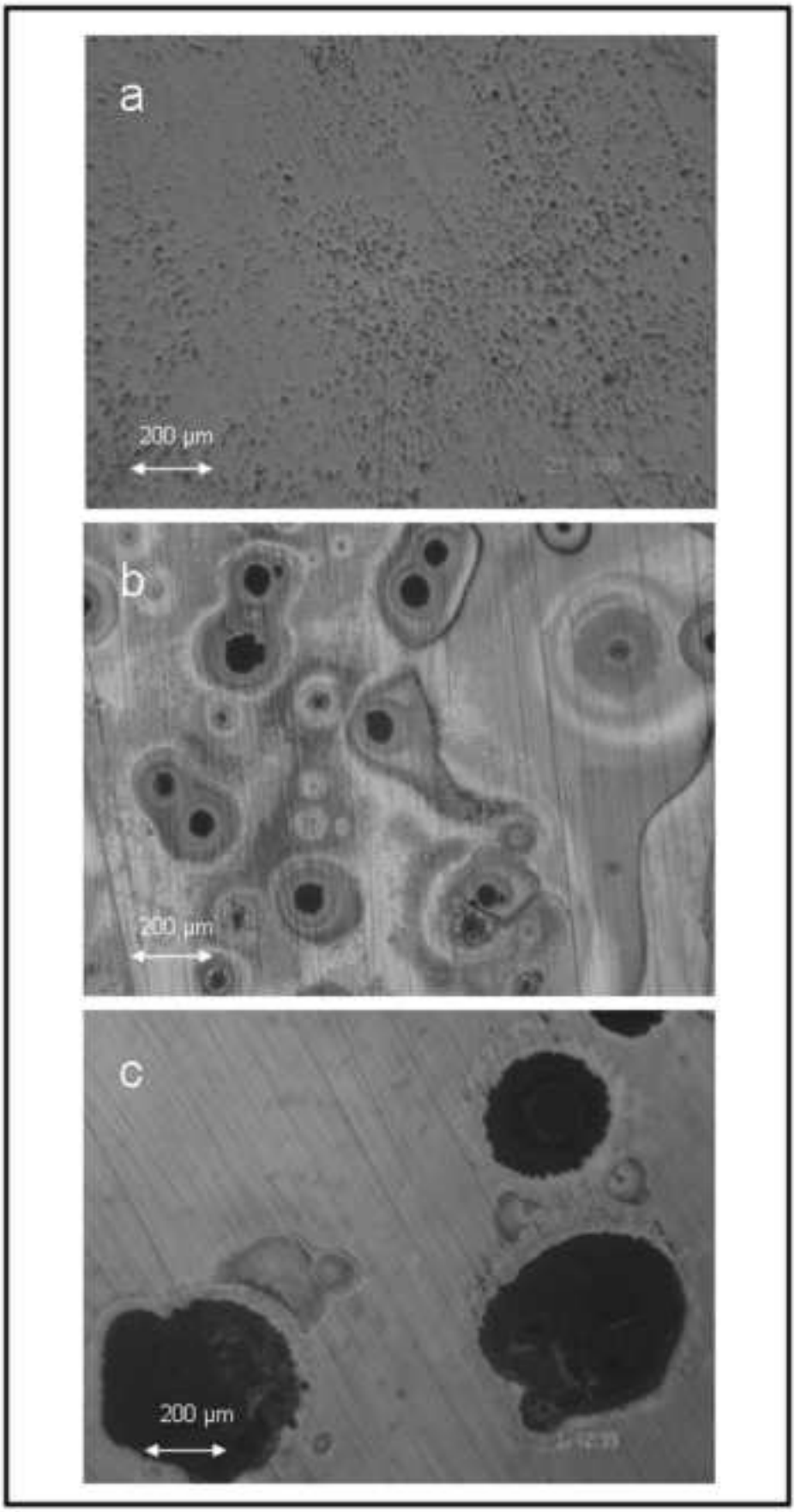

Table 1. Optimised values for the parameters employed in fitting the data in Figs. 8 a, b y c with the equivalent circuit proposed in Fig. 1.

Element	ATW	ATW + 5 mg l^{-1} P	ATW + 10 mg l^{-1} P
Rs/Ω cm^2	374	223	177
Qo/μΩ^{-1} cm^{-2} S^n	24.4	16.8	19.8
***n*o**	0.82	0.81	0.81
Ro/kΩ cm^2	1.2	10.9	14.2
Qdl/μΩ^{-1} cm^{-2} S^n	126	33.4	28.8
n_{dl}	0.56	0.5 (fixed)	0.5 (fixed)
R_{dl}/kΩ cm^2	25.4	117.4	137.6

Table 2. Relevant average values, of at least three independent measurements, of electrochemical parameters that characterise the anodic polarisation curves on brass. The scan direction is reversed at 0.218 mA cm^{-2}.

	ATW	**ATW + 5 mg l^{-1} P**	**ATW + 10 mg l^{-1} P**
E_p /mV$_{SCE}$	-5 ± 15	53 ± 11	141 ± 21
E_{corr} /mV$_{SCE}$	-50 ± 5	-79 ± 10	-65 ± 18
E_p-E_{corr}	55 ± 13	138 ± 15	215 ± 30
E_{rp} /mV $_{SCE}$	-26 ± 94	-36 ± 10	-15 ± 4
E_p-E_{rp}	26 ± 21	91 ± 9	167 ± 14
E_{rp}-E_{corr}	24 ± 4	47 ± 7	49 ± 20

Table 3. Average of polarization resistance values, evaluated from at least three independent measurements, for brass held for 2 hours in ATW, ATW + 5 mg l^{-1} P and ATW + 10 mg l^{-1} P at E_{corr}. Rp_{sweep} are polarization resistance measurements from potential sweeps in the vicinity of the E_{corr} and Rp_{EIS} (R_{dl}) are calculated after fitting EIS results to the equivalent circuit in Fig. 1.

	Rp_{sweep} kΩ cm^2	**Rp_{EIS} kΩ cm^2**
ATW	23.8 ± 2.4	27.6 ± 3.2
ATW + 5 mg l^{-1} P	88.4 ± 12.1	110.2 ± 32.0
ATW + 10 mg l^{-1} P	102.0 ± 31.9	141.5 ± 26.3

- Brass in contact with tap water is covered by Zn (II) oxide-hydroxide and Cu_2O.

- With PO_4^{3-} as corrosion inhibitor, the film becomes less porous, thinner and denser.

- The optimal dose of inhibitor required is 10 mg l^{-1} P